Applied Catalysis B: Environmental 170-171 (2015) 255–262

Contents lists available at ScienceDirect

Applied Catalysis B: Environmental

journal homepage: www.elsevier.com/locate/apcatb

Visible-light-mediated synergistic photocatalytic antimicrobial effects and mechanism of Ag-nanoparticles@chitosan–TiO_2 organic–inorganic composites for water disinfection

Gang Xiao, Xi Zhang, Wanying Zhang, Shan Zhang, Haijia Su*, Tianwei Tan

Beijing Key Laboratory of Bioprocess, Beijing University of Chemical Technology, Beijing 100029, PR China

ARTICLE INFO

Article history:
Received 7 November 2014
Received in revised form 30 January 2015
Accepted 31 January 2015
Available online 2 February 2015

Keywords:
Ag nanoparticles@chitosan–TiO_2
Visible light irradiation
Photocatalytic antimicrobial activities
Antimicrobial mechanism
Water disinfection

ABSTRACT

By coupling chitosan bioaffinity adsorption, molecular imprinting, and nano TiO_2 photocatalysis technologies, Ag nanoparticles@chitosan–TiO_2 organic–inorganic composite (Ag-NPs@CTA) was prepared and found to be an efficient visible-light-mediated photocatalytic antimicrobial agent useful for water disinfection. Ag-NPs@CTA exhibited favorable antimicrobial activity for *Escherichia coli*, *Staphylococcus aureus* and *Candida albicans*, with the inactivation rate in excess of 99.0% in 2 h under visible light irradiation. Ag-NPs@CTA could be reused for five consecutive cycles directly without regeneration treatment and showed rather low cytotoxicity toward mammalian cells. Characterization of *E. coli* cells using TEM, AFM, Raman spectroscopy, FTIR and intracellular protein leakage illustrated that Ag-NPs@CTA could not only destroy the cell wall and membrane but also cause metabolic dysfunction. The synergistic antimicrobial mechanism was studied by Ag release evaluation, radical scavengers study, and Ag-NPs@CTA characterization by XPS and UV–vis absorption. The enhanced antimicrobial ability originated from the synergistic activities of the three components and the proposed mechanisms contained electrostatic interaction followed by two pathways: released Ag species and oxidative stress caused by photo-generated reactive radicals. The present work provided an efficient water disinfection technology of realistic potential and also opened a new idea in designing visible-light-mediated photocatalytic antimicrobial agents and in studying the antimicrobial mechanism.

1. Introduction

Over 15% of the world population (about 1.2 billion) lack access to safe potable water which is the fundamental necessity for the sustainable development of our human society [1]. Water resource contamination has been a serious social and worldwide problem, especially for less developed countries and causing millions of death annually [2]. Pathogenic microorganisms (e.g., *Escherichia coli*, *Vibrio cholerae*, *Salmonella* spp.) are high threats to human health and have caused water-borne diseases such as diarrhea, cholera, septicemia, gastroenteritis, etc. [3,4]. So, it is essential to conduct disinfection to produce clean potable water [5].

Conventional chemical disinfection processes using free chlorine, chloramines and ozone have been proven effective in controlling microbial pathogens [6,7]. However, these chemical disinfection agents can react with various natural organic compounds in water to form more than 600 known harmful disinfection byproducts (DBPs), some of which have been identified as carcinogenic and mutagenic [8–11]. UV irradiation is less effective because of its limited penetration in water and UV itself is harmful and energy-intensive [8,12]. Although, antibiotics are commonly used to inhibit the growth of pathogenic microorganisms, they can lead to the emergence of multi-resistance and are also not recommended [13]. Therefore, it is of paramount importance to develop an innovative antimicrobial agent to provide a reliable and robust disinfection method.

Titanium dioxide (TiO_2) has been considered as the most promising photocatalyst for widespread environmental applications because of its high reactivity, high chemical stability, biocompatibility and inexpensive commercial availability [14–16]. Since Matsunaga et al. [17] first reported the photochemical sterilization ability of platinized TiO_2 for *Lactobacillus acidophilus*, *Saccharomyces cerevisiae* and *Escherichia coli*, light-mediated TiO_2 photocatalytic antimicrobial targeting various pathogens such as

* Corresponding author at: College of Life Science and Technology, P.O. Box 53, Beijing Key Laboratory of Bioprocess, Beijing University of Chemical Technology, Beijing 100029, PR China. Tel.: +86 10 64452756; fax: +86 10 64414268.
E-mail address: suhj@mail.buct.edu.cn (H. Su).

http://dx.doi.org/10.1016/j.apcatb.2015.01.042
0926-3373/

bacteria, fungi and viruses has received noticeable interest from researchers [18,19].

However, the photocatalytic antimicrobial ability of pure TiO_2 is valid only under UV light irradiation owing to its wide band gap energy of 3.2 eV [20]. Considering the utilization and conversion of abundant solar energy, silver nanoparticles, which can generate free electrons under visible light irradiation because of surface plasmonic resonance (SPR) effect, have been successfully used to make TiO_2 more active in visible light region [21–23]. Silver nanoparticles deposition is also beneficial for the photocatalysis process of TiO_2 because the incorporation of Ag onto a TiO_2 surface can enhance the interfacial charge transfer and restrict the electron-hole recombination [24,25]. Furthermore, silver itself has been recognized as a natural antimicrobial agent since ancient times and silver can also act as an antimicrobial auxiliary agent as deposit on a TiO_2 surface [26].

Another significant drawback of TiO_2 powder for water disinfection applications is the non-reusability because it is very difficult to recover the suspended TiO_2 from water [27]. Immobilization using various polymer substances such as polyvinyl alcohol, polyvinyl chloride, polyvinyl acetate, chitosan and cellulose has been proven to be a promising method to solve this problem and the obtained organic–inorganic composites exhibit combined and superadditive characters from both organic and inorganic materials [28–31]. Among these supporting polymers, chitosan (linear and partly acetylated (1-4)-2-amino-2-deoxy-β-D-glucan is preferred because it is naturally abundant, nontoxic and biodegradable and can also inhibit the growth of bacteria and fungi [32–34]. Furthermore, the existence of polycationic chitosan is beneficial for TiO_2 or other inorganic nanoparticles binding to the negatively charged cell surface through electrostatic interaction [35].

In our previous work, well dispersed Ag nanoparticles (Ag-NPs) were prepared onto the surface active imprinting sites of chitosan–TiO_2 adsorbent (CTA) through the coupling of chitosan bioaffinity adsorption, molecular imprinting and nano TiO_2 photocatalysis technologies and the antimicrobial properties of the prepared Ag nanoparticles were preliminarily studied [36]. However, we just focused on the silver nanoparticles at that time and did not realize the potential synergistic effects of Ag nanoparticles@chitosan–TiO_2 inorganic–organic composite (Ag-NPs@CTA) on microbial cells. In the present paper, we found light resource to be an important factor influencing the antimicrobial activities and recognized Ag-NPs@CTA as an efficient visible-light-mediated photocatalytic antimicrobial agent useful in water disinfection. Antimicrobial properties of Ag-NPs@CTA in water were studied in detail by evaluating the influences of the key factors including microbial type, initial microbial concentration, light source and time. The reusability and cytotoxicity toward mammalian cells were also investigated considering its realistic applications in drinking water disinfection. Then, the influences of Ag-NPs@CTA treatment on microbial cell structure and substances were studied by the characterization of *E. coli* cells using TEM, AFM, Raman spectroscopy, FTIR and intracellular substances leakage. Finally, the synergistic mechanism of the visible-light-mediated antimicrobial activity of Ag-NPs@CTA toward microbial cells was discussed in detail.

2. Experimental

2.1. Chemicals and materials

Chitosan with 85.0% degree of deacetylation was purchased from Jinan Haidebei Marine Bioengineering Co., Ltd. (Jinan, China). Titanium dioxide (Degussa P25, 80% anatase, 20% rutile, 50 $m^2\ g^{-1}$, primary particle size ~25–30 nm, agglomerate size ~100 nm) was used in this work. $AgNO_3$, $NiSO_4{\cdot}6H_2O$, EDTA-2Na, NaOH, NaCl, acetic acid, epichlorohydrin, *t*-butanol, ammonium oxalate, and benzoquinone were of analytical grade and purchased from Beijing Chemical Works (China). Catalase lyophilized powder (≥10,000 units mg^{-1} protein) was purchased from Sigma–Aldrich. Beef peptone, beef extract powder, yeast extract powder, glucose and agar were of biochemical grade and purchased from Beijing AoBoXing Bio-Tech Co., Ltd. (China). Deionized water was used throughout all the experiments.

2.2. Synthesis of Ag nanoparticles@chitosan–TiO_2 organic–inorganic composites (Ag-NPs@CTA)

The preparation method of imprinting chitosan–TiO_2 adsorbents (CTA) was described in our previous paper [36]. Ag nanoparticles were synthesized on the surface active sites of CTA through the following process: 0.15 g CTA was added into 40 mL $AgNO_3$ aqueous solution (Ag^+ mass concentration 200 mg L^{-1}); then, the mixtures were shaken for 2 h in a reciprocal shaker (agitation rate 80 rpm) under ultraviolet irradiation (a UV-A lamp of 40 W with irradiation wavelength peak at 365 nm) at room temperature. Well dispersed Ag nanoparticles could be obtained on the surface of CTA with average diameter of 50 nm (Fig. S1). The obtained loading capacity of Ag nanoparticles on CTA was calculated to be 16.96 mg g^{-1} by monitoring the Ag^+ mass concentration changes in the solution. And the mass fraction of Ag nanoparticles for the synthesized Ag-NPs@CTA was 1.67 wt%.

2.3. Synergistic antimicrobial properties of Ag-NPs@CTA

Escherichia coli (ATCC 8099), *Staphylococcus aureus* (ATCC 6538) and *Candida albicans* (ATCC 10,231), obtained from the American Type Culture Collection, were chosen as the three test strains. The initial concentration of the microbiological cells was determined using the spread plating colony enumeration method [37]. The typical antimicrobial experiment methods were as following: four particles of Ag-NPs@CTA (3.0 mg) were immersed in 10 mL microbiological cell suspension with predetermined initial colony forming unit (CFU); then, the mixtures were incubated in a shaking incubator at 37 °C for 15–180 min under visible light irradiation (20 W fluorescent lamp); after a certain time, the final CFU was determined using the spread plate technique with three parallel enumeration tests for each assay. For the antimicrobial experiments under UV irradiation, a 20 W UV-A lamp with central wavelength of 365 nm was used. Whereas for the antimicrobial agents reuse experiments, Ag-NPs@CTA particles were recovered from the cell suspension and washed with 5 mL of sterilized 0.85% saline; then, these particles were reused directly for the next antimicrobial cycle without further regeneration processes. All the experiments mentioned above were carried out in triplicate and the average values were reported.

2.4. In vitro cytotoxicity assay

Cytotoxicity of Ag-NPs@CTA toward mammalian cells was evaluated according to State Standard of the People's Republic of China (GB/T 16,886.5-2003, Biological evaluation of medical devices Part 5: test for in vitro cytotoxicity) using Vero cells. Ag-NPs@CTA was first immersed into sterilized 0.85% saline and incubated at 37 °C for 24 h to obtain the leaching solution for cytotoxicity test. Then the original leaching solution was diluted for 2 times, 4 times and 8 times and the diluted solution with different concentrations was recognized as 1/2, 1/4 and 1/8 leaching solution, respectively. Vero cells were treated with various leaching solutions at 37 °C for 24 h and the cell viabilities were analyzed for five parallel tests using

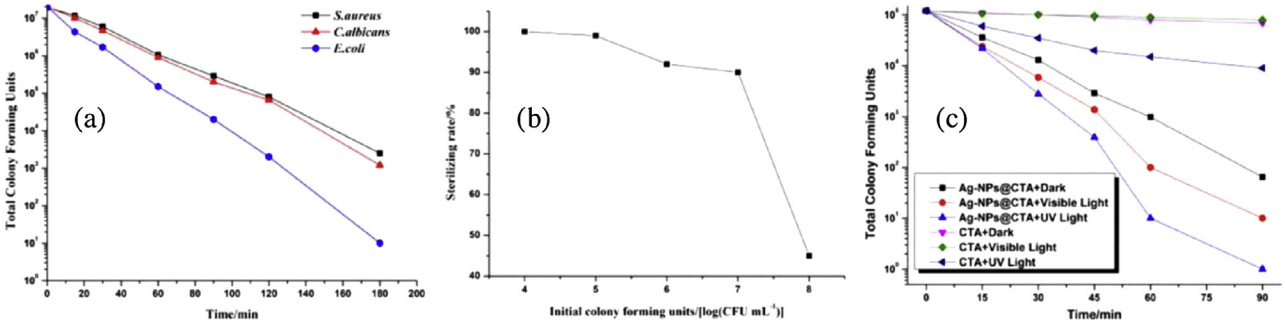

Fig. 1. (a) Antimicrobial kinetics of Ag-NPs@CTA for *E. coli*, *S. aureus* and *C. albicans*. (b) Sterilizing rate of *E. coli* under different initial colony forming units using Ag-NPs@CTA within 1 h. (c) Antimicrobial kinetics of Ag-NPs@CTA and CTA against *E. coli* under different light sources.

MTT assay as described [35]. The cells treated with sterilized deionized water were set as the positive control (proliferation rate set to 100%). The cell morphologies of control group and original leaching solution treatment group were also recorded using a camera equipped optical microscope.

2.5. Cells structures characterization using AFM and TEM

E. coli cells (10^9 CFU mL^{-1}) were treated with Ag-NPs@CTA for different times using the typical antimicrobial experiment method mentioned above. Then, the cells were collected and washed twice with PBS, followed by fixing with 2.5% glutaraldehyde overnight. The fixed samples were dehydrated with sequential treatments by 30%, 50%, 70%, 80%, 90%, and 100% ethanol for 10 min, respectively. Finally, the cells suspension was dropped on a carbon coated copper grid for TEM and a clean mica sheet for AFM, and then thoroughly dried under N_2 gas. VEECO Multimode 8, operating in scan mode, was used for AFM imaging and analysis using the following method: (1) in order to locate on the cell surface, a 5 μm × 5 μm square area which contained several *E. coli* cells were chosen for scan; (2) then, we focused on a 1 μm × 1 μm square area with a single cell in the center and chose five 250 nm × 250 nm square area randomly for the cell surface roughness analysis for each sample. The dried samples were also observed using a transmission electron microscopy (Hitachi H800, Tokyo, Japan).

2.6. E. coli intracellular protein leakage analysis

Protein content in supernatants released from *E. coli* cells was determined in order to evaluate the membrane integrity. *E. coli* cells (10^9 CFU mL^{-1}) were treated with Ag-NPs@CTA for different times using the typical antimicrobial experiment method mentioned above. The samples were centrifuged at 10,000 × *g* (4 °C, 10 min) to obtain the supernatants which were analyzed using a modified Coomassie brilliant blue assay (Bradford method) to determine the amount of protein released from the cells [38]. The experiments were carried out in triplicate and the average values were reported.

2.7. Cells substances analysis by Raman spectroscopy and FTIR

E. coli cells (10^9 CFU mL^{-1}) were treated with Ag-NPs@CTA for 180 min using the typical antimicrobial experiment method mentioned above. 10 mL cells suspension was centrifuged at 10,000 × *g* (4 °C, 10 min) to remove the broth and then the obtained cells were resuspended in deionized water. Then, the cells suspension was concentrated by repeating the centrifugation–resuspension processes until the volume of the cells suspension reached to 1 mL. *E. coli* cells suspension without Ag-NPs@CTA treatment was also prepared using the same method. For Raman spectroscopy analysis, 20 μL of the cells suspension was dropped onto the N-type (1 0 0) Si wafer substrate (sequentially cleaned in deionized water, acetone, and alcohol for 5 min each before use) and dried under N_2 gas. This step was repeated for another four times to obtain the proper sample thickness. A LabRAM Aramis Raman system (HORIBA Jobin Yvon) was used for Raman spectra acquisition. He–Ne 785 nm line laser with the power of 3 mW and spot size of 1 μm was used as excitation source. The spectra were recorded with an accumulation time of 5 s in the region of 400 to 1800 cm^{-1} at 1 cm^{-1} spectral resolution. For each sample, five spectra were collected from different spots to ensure the reproducibility. For FTIR analysis, the samples were centrifuged and the wet bacteria were dried at 30 °C for 24 h. FTIR analyses were performed on KBr discs with a 2% finely ground sample (dried bacteria sample 1 mg with KBr 100 mg), analyzed in a Varian 3100 FTIR spectrometer and the infrared spectra of *E. coli* cells before and after treatment with Ag-NPs@CTA were recorded in the wavenumber region of 4000–400 cm^{-1} at 2 cm^{-1} spectral resolution.

2.8. Ag release test and pH changes evaluation

E. coli cells suspension (10^7 CFU mL^{-1}, diluted with sterile 0.85% saline or sterile water) was treated with 3.0 mg Ag-NPs@CTA for different times under visible light irradiation using the typical antimicrobial experiment method mentioned above. During the antimicrobial process, the total Ag concentration was measured at different times by an atomic absorption spectrophotometer (Varian SpectrAA55-B, Palo Alto, USA). The total Ag concentration in the sterile 0.85% saline and sterile water under the same conditions at different times was also recorded for comparison. For pH change evaluation, *E. coli* cells suspension (10^9 CFU mL^{-1}) was treated with 0.06 g Ag-NPs@CTA under visible light irradiation using the typical antimicrobial experiment method mentioned above and a desktop pH meter (METTLER TOLEDO, FE20-FiveEasy^{TM}) was used to record the pH changes during the antimicrobial process. *E. coli* cells suspension without Ag-NPs@CTA and Ag-NPs@CTA in the sterilized 0.85% saline were set as the two control groups and the pH values at different times were measured for comparison.

2.9. Radical scavenger study

Four radical scavengers, *t*-butanol (0.1 M), ammonium oxalate (0.1 M), catalase (100 units mL^{-1}), and benzoquinone (0.1 M) were employed to study the presence of hydroxyl radicals, photogenerated holes, H_2O_2, and superoxide radicals, respectively. 1 mL of scavenger was added into 9 mL of *E. coli* suspension (10^5 CFU mL^{-1}) and the mixed solution was used for antimicrobial test using the typical method mentioned in Section 2.3 for 90 min under visible light irradiation. 1 mL of sterile 0.85% saline was added for the control experiment without scavenger.

Table 1
Specific death rate of Ag-NPs@CTA against *E. coli* with different light sources

	CTA			Ag-NPs@CTA		
	Dark	Visible light	UV light	Dark	Visible light	UV light
The specific death rate constant k(CFU min^{-1})	0.00269	0.00182	0.01244	0.03671	0.04341	0.05960
Correlation coefficient	−0.99611	−0.98421	−0.97645	−0.99946	−0.99438	−0.98929

2.10. Ag-NPs@CTA characterization

X-ray photoelectron spectra (XPS) analysis for CTA and Ag-NPs@CTA was carried out using an ESCALAB 250 instrument (Thermo Fisher Scientific) with Al Kα irradiation and the C (1s) level (285.0 eV) was taken as the reference binding energy. UV–vis absorption spectroscopy analysis for CTA and Ag-NPs@CTA (prepared as membranes coated on the surface of quartz cuvette using the same method) was performed on a Cary 100 Bio UV–vis spectrophotometer (Varian SpectrAA55-B, Palo Alto, USA).

3. Results and discussion

3.1. Synergistic antimicrobial properties of Ag-NPs@CTA

In order to evaluate the applicability of Ag-NPs@CTA in water disinfection, the antimicrobial activities for three test strains *E. coli* (gram-negative bacteria), *S. aureus* (gram-positive bacteria) and *C. albicans* (fungi) were studied and the results were shown in Fig. 1a. As can be seen in Fig. 1a, after 2 h of sterilizing, the antimicrobial rates of the three strains were all in excess of 99.0% which illustrated that Ag-NPs@CTA possessed efficient antimicrobial activities for both bacteria and fungi. The specific death rate constants (k) of *E. coli*, *S. aureus* and *C. albicans* were calculated to be 0.034 CFU min^{-1}, 0.021 CFU min^{-1} and 0.023 CFU min^{-1}, respectively. Ag-NPs@CTA showed relatively higher antimicrobial activity for *E. coli* than for *S. aureus* and *C. albicans* because gram-negative bacteria had thinner cell wall than gram-positive bacteria and fungi and it is easier for Ag-NPs@CTA to destroy the cell membrane of *E. coli* and cause cell death [39,40].

Initial concentration of microorganism cells is another significant factor influencing the overall antimicrobial efficiency. Ag-NPs@CTA sterilization for *E. coli* with different initial CFUs was conducted and the results were shown in Fig. 1b. As shown in Fig. 1b, when the initial bacteria concentration was less than 10^8 CFU mL^{-1}, the sterilizing rate for *E. coli* could keep at a rather high level and did not change obviously. However, when the initial bacteria concentration reached 10^8 CFU mL^{-1}, the bactericidal rate saw a significant decreasing to less than 50% within 1 h. This is because the light absorption of the cell suspension could not be ignored under high concentration while the light was the main energy input for photocatalytic antimicrobial activity of Ag-NPs@CTA. So, the overall sterilizing rate for *E. coli* decreased with increasing the initial microbial cell concentration, especially under high CFUs.

To further understand the synergistic antimicrobial effects of Ag-NPs@CTA, the influences of light source on the antimicrobial activities of Ag-NPs@CTA and CTA against *E. coli* were studied. The antimicrobial kinetics results were shown in Fig. 1c and the specific death rate constants (k) were calculated as shown in Table 1. CTA showed slight antimicrobial activities mainly from positively charged chitosan in the case of visible light and dark conditions because TiO_2 could only be activated by UV light. However, under UV irradiation, CTA showed enhanced antimicrobial activity for *E. coli* because UV could activate TiO_2 to generate OH• which was highly destructive to bacterial cells [12,20]. Furthermore, UV light itself could also contribute to kill bacterial cells (k = 0.0018 CFU min^{-1} for UV control experiment without antimicrobial agent), although it did not play a major role in the antimicrobial effects. After deposition of Ag-NPs, the antimicrobial agent showed much higher sterilizing efficiency (k = 0.037 CFU min^{-1}) even without light, which proved that Ag-NPs could play an important role independently in the bactericidal effect of Ag-NPs@CTA. When visible light was introduced, the antimicrobial activity of Ag-NPs@CTA was further enhanced (k = 0.043 CFU min^{-1}) because Ag-NPs could absorb visible light to generate free electrons which could transfer to the neighbor TiO_2 to trigger charge separation and subsequent photocatalytic reactions [22,23]. While under UV light condition, Ag-NPs@CTA performed the best antimicrobial activity (k = 0.060 CFU min^{-1}) because UV light could not only enhance the photocatalytic activity of Ag-NPs doped TiO_2 but also possessed sterilization ability itself.

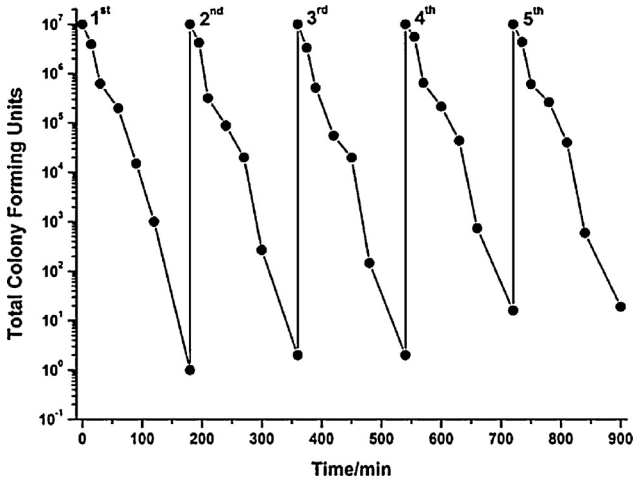

Fig. 2. Reusability of Ag-NPs@CTA for water disinfection (*E. coli* as test strain) under visible light irradiation.

3.2. Reusability of Ag-NPs@CTA

Considering the realistic application of Ag-NPs@CTA for the disinfection of drinking water, the reusability was further evaluated using *E. coli* as test strain (Fig. 2). Ag-NPs@CTA particles were recovered and washed with sterilized 0.85% saline, and then the antimicrobial particles were reused directly for destruction of *E. coli* without regeneration treatment. Ag-NPs@CTA could be successfully reused for five consecutive cycles without significant decrease in antimicrobial efficiency (all the microbial inactivation rates during the five cycles were higher than 99.99%). The reusability of Ag-NPs@CTA could save the cost obviously, thus facilitating the realistic application for water disinfection.

3.3. In vitro cytotoxicity evaluation

Cytotoxicity evaluation for the antimicrobial agent toward mammalian cells is essential for its application in drinking water purification. The viabilities of Vero cells after treatment with Ag-NPs@CTA leaching solutions were analyzed using MTT assay (Fig. S2). The cell viability was over 92% even for the original leaching

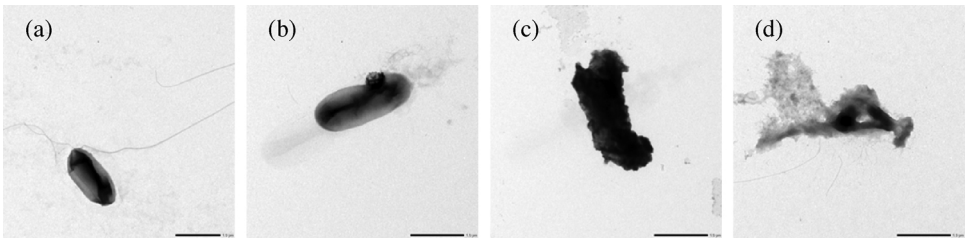

Fig. 3. TEM micrographs of *E. coli* cells after treatment with Ag-NPs@CTA for different times: (a) 0 min. (b) 60 min. (c) 120 min. (d) 180 min.

solution and the cellular morphology did not show significant different between the control group and the original leaching solution treating group. The results indicated that Ag-NPs@CTA had low toxicity toward mammalian cells and was promising as antimicrobial agent for drinking water purification.

3.4. Cells structure damage after treatment with Ag-NPs@CTA

As discussed above, Ag-NPs@CTA was proven to be a promising antimicrobial agent for water disinfection application. Then we tried to explain how the microbial cells were killed by studying the cells changed during contacting with Ag-NPs@CTA. Firstly, the influences of Ag-NPs@CTA treatment on the cell morphology and structure were studied in this section.

The morphology changes of *E. coli* cells contacting with Ag-NPs@CTA for different times were first examined by TEM (Fig. 3). Before contact with Ag-NPs@CTA, *E. coli* cells kept their intact structure and smooth surface (Fig. 3a), while after 60 min, the cells structure became deformed on some sites of the cell surface (Fig. 3b). When the treatment time with Ag-NPs@CTA was prolonged to 120 min, the cells were obviously damaged with rough appearance on a disorganized cell surface (Fig. 3c). The cells were nearly broken down to debris after treatment with Ag-NPs@CTA for 180 min and the leakage of intracellular contents could be observed (Fig. 3d). These results indicated that the bacteria were thoroughly killed other than inhibited by the destruction of cell wall and membrane and the resulting intracellular substances release, in agreement with previous reports [23,41].

In order to further evaluate the cells structure changes, cells imaging and roughness analysis was conducted using AFM which has been proven to be a suitable tool for the observation of cells morphology and structure changes [42]. AFM cells imaging results (Fig. S3) clearly showed that *E. coli* cells became rougher contacting with Ag-NPs@CTA and finally sagged obviously after 180 min illustrating the integrity of cells had been destroyed. The average cell surface roughness increased form 2.12 nm to 6.06 nm after contacting with Ag-NPs@CTA for 180 min (Table S2) resulting from the fine structure changes of cell wall and membrane. AFM analysis results indicated that Ag-NPs@CTA could cause serious damage to the bacterial surface structure and lead to the loss of cell integrity which agreed with the TEM characterization results.

In order to verify the cells damage and resulted intracellular substances leakage illustrated by TEM images (Fig. 3), protein leakage from *E. coli* cells was determined after contacting with Ag-NPs@CTA for different times (Fig. S4). In the first 60 min, intracellular protein leakage increased dramatically to 2750 $\mu g\,mL^{-1}$ because of the cell membrane permeability disorder resulting from the treatment of Ag-NPs@CTA. Then, the protein leakage increased slowly and reached to relatively steady values with further destruction and final cracking of cell membrane. The protein leakage analysis results indicated clearly that Ag-NPs@CTA treatment under visible light irradiation would cause cell death with thorough cracking of cell wall and membrane, inconsistent with TEM and AFM analysis results.

3.5. Cells substances change after treatment with Ag-NPs@CTA

In order to understand the antimicrobial mechanism in the substance metabolism level, we try to study the cells substances changes with Ag-NPs@CTA treatment using Raman spectroscopy and FTIR analysis. The Raman spectra of *E. coli* cells before and after treatment with Ag-NPs@CTA were recorded (Fig. S5) and the main peaks were assigned to the corresponding substances or groups (Table S3) according to the literatures [43–48]. From the comparison between the two Raman spectra, three obvious changes could be concluded: (1) the peaks changes at 572.0 cm^{-1}, 932.6 cm^{-1} and 1023.3 cm^{-1} indicated that Ag-NPs@CTA would influence the substances such as carbohydrates, phospholipids present in cell wall and cell membrane; (2) peaks at 833.7 cm^{-1}, 1219.8 cm^{-1} and 1359.3 cm^{-1} illustrated the changes of cells proteins; (3) nucleic acid related peaks changes at 648.8 cm^{-1}, 725.6 cm^{-1}, 1081.4 cm^{-1} and 1623.3 cm^{-1}. The Raman analysis results indicated that Ag-NPs@CTA could not only damage the cell wall and cell membrane (in agreement with the TEM and AFM analysis results) but also affect the substances metabolism which was performed by proteins and controlled by nucleic acid. Then FTIR was used for the

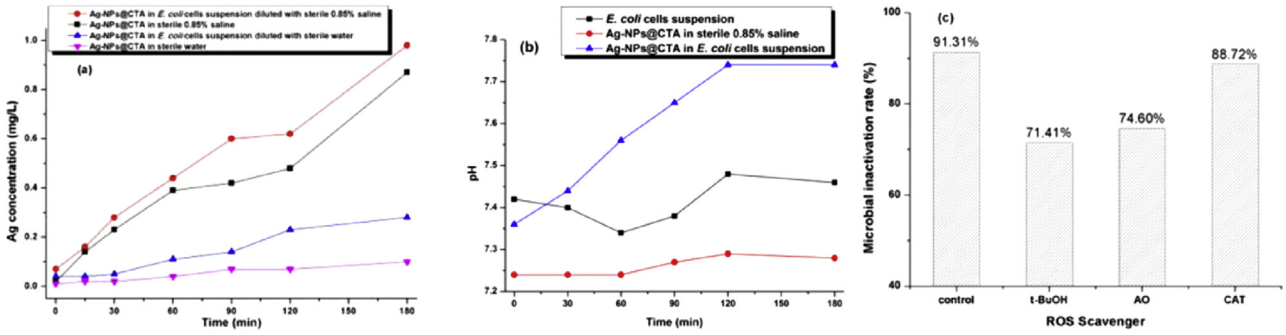

Fig. 4. (a) Ag release in *E. coli* cells suspension diluted with sterile 0.85% saline and sterile water (blank sterile 0.85% saline and sterile water as control experiments). (b) pH changes in *E. coli* cells suspension after contacting with Ag-NPs@CTA for different time (*E. coli* cells suspension without Ag-NPs@CTA and Ag-NPs@CTA in sterile 0.85% saline as control experiments). (c) Effects of different ROS scavengers on the antimicrobial activity of Ag-NPs@CTA against *E. coli* for 90 min.

cells substances characterization and the results were shown in Fig. S6 with the main absorption bands assignment was shown in Table S4 according to the literatures [49–51]. Absorption band changes clearly illustrated that Ag-NPs@CTA could affect the cellular substances containing carbohydrates, proteins and P containing molecules during the antimicrobial process under visible light irradiation, in consistent with Raman spectroscopy characterization.

3.6. Synergistic antimicrobial mechanism of Ag-NPs@CTA

The antimicrobial ability of Ag-NPs@CTA originates from the synergistic activities of the three components, i.e., chitosan, TiO_2 and Ag nanoparticles. The corresponding activities of different components of Ag-NPs@CTA under visible light irradiation were studied in order to investigate the synergistic antimicrobial mechanism of Ag-NPs@CTA and the results were shown in Fig. S7. Under visible light, pure chitosan and TiO_2 did not show antimicrobial activities against *E. coli* cells because chitosan could only prevent the growth of microbial cells by electrostatic attraction rather than kill them, while TiO_2 could not be activated by visible light. After Ag nanoparticles loading, the antimicrobial activity of both Ag-NPs@chitosan and Ag-NPs@TiO_2 was enhanced obviously although still lower than that of Ag-NPs@CTA. The obvious difference of antimicrobial activity between pure chitosan and Ag-NPs@chitosan illustrated that Ag nanoparticles could contribute to inactive microbial cells independently, while the enhanced activity of Ag-NPs@TiO_2 compared with pure TiO_2 originated form the visible light mediated photocatalysis effects. When compared with Ag-NPs@TiO_2, Ag-NPs@chitosan showed a little higher activity toward *E. coli*, possibly because Ag-NPs@chitosan could easily bind to the surface of microbial cells by electrostatic interaction.

Firstly, the contribution of Ag nanoparticles for the antimicrobial activity of Ag-NPs@CTA was studied. Free silver (as Ag^+ or Ag-NPs/Ag^+) could be released from the surface loaded Ag nanoparticles and showed antimicrobial activities independently through the three possible mechanisms: Ag^+ or Ag-NPs/Ag^+ could (i) bind to the cell membrane to alert its natural permeability and other functions [52]; (ii) interact with thiols in proteins and lead to metabolic disorders, for example, bind to enzymes which are involved in the bacterial respiratory chain and cause intracellular oxidative stress [53,54]; (iii) interact with phosphorus moieties of DNA, thereby inactivating its replication process through preventing DNA from unwinding [55]. In order to verify the antimicrobial activity of Ag nanoparticles, silver release in *E. coli* cells suspension (diluted with sterile 0.85% saline) and sterile 0.85% saline (as control) were evaluated as shown in Fig. 4a. The free silver concentration increased gradually in both *E. coli* cells suspension and sterile 0.85% saline, and silver release in *E. coli* cells suspension was higher than that in sterile 0.85% saline illustrating that free silver ions could bind to the outer surface or penetrate into the cells. The above results proved that Ag nanoparticles could trigger antimicrobial effects independently by releasing free silver species. Furthermore, in order to evaluate the potential cytotoxicity of Ag-NPs@CTA, sterile water was used to dilute *E. coli* cells suspension because chloride ions in saline would promote the release of free silver species by forming insoluble silver chloride. As can be seen from Fig. 4a, the free silver concentration was rather low in sterile water (less than 0.1 mg L^{-1}). The results indicated that Ag-NPs@CTA was promising as antimicrobial agent for drinking water purification which was inconsistent with the in vitro cytotoxicity evaluation results using MTT method (Section 3.3).

In order to study the visible light mediated synergistic photocatalytic antimicrobial mechanism, pH changes during the disinfection of Ag-NPs@CTA toward *E. coli* were recorded as shown in Fig. 4b. When compared with the two control experiments, i.e., *E. coli* cells suspension without Ag-NPs@CTA treatment and Ag-NPs@CTA in sterile 0.85% saline, pH of the cells suspension increased obviously after treatment with Ag-NPs@CTA under visible light irradiation from 7.36 to 7.74 and kept stable after 120 min. This could be resulted from the generation of reactive oxygen species ($O_2^{\bullet -}$, $HO_2^{\bullet}$, H_2O_2, and $OH^{\bullet}$) and hydroxyl ions (OH^-) by consuming dissolved oxygen and protons (H^+) during the visible light mediated photocatalysis processes. The relevant reactions could be expressed as follows:

$$Ag@TiO_2 + h\nu \rightarrow e^- + h^+ \quad (1)$$

$$e^- + O_2 \rightarrow O_2^{\bullet -} \quad (2)$$

$$4O_2^{\bullet -} + H^+ \rightarrow HO_2^{\bullet} \quad (3)$$

$$e^- + O_2^{\bullet -} + 2H^+ \rightarrow H_2O_2 \quad (4)$$

$$2e^- + HO_2^{\bullet} + H^+ \rightarrow OH^{\bullet} + OH^- \quad (5)$$

$$h^+, H_2O_2, O_2^{\bullet -}, OH^{\bullet}, HO_2^{\bullet} + E.coli\text{cells} \rightarrow \text{inactivated}E.coli\text{cells} \quad (6)$$

Then, the effects of different reactive oxygen species (ROSs) scavengers on the antimicrobial activity of Ag-NPs@CTA against *E. coli* cells were studied in order to indicate the role of ROSs in the microbial inactivation process using *t*-butanol (*t*-BuOH), ammonium oxalate (AO), catalase (CAT), and benzoquinone (BQ) as the scavenger of hydroxyl radicals ($OH^{\bullet}$), photo-generated holes (h^+), H_2O_2, and superoxide radicals ($O_2^{\bullet -}$ and $HO_2^{\bullet}$), respectively [56–58]. The microbial inactivation rates of Ag-NPs@CTA for *E. coli* cells after different scavengers were introduced were recorded as shown in Fig. 4c (result of benzoquinone addition was not shown because it is highly toxic toward *E. coli* cells and no colony of *E. coli* existed after benzoquinone was introduced). As can be seen from Fig. 4c, the antimicrobial activity of Ag-NPs@CTA against *E. coli* decreased obviously when *t*-butanol or ammonium oxalate was introduced illustrating the contribution of $OH^{\bullet}$ and h^+ to the microbial inactivation effects. However, when the scavenger catalase was added into the system, the microbial inactivation rate only showed a slight decrease compared with that of the control experiment without scavenger indicating that H_2O_2 was not the main reactive oxygen species. Furthermore, because both $OH^{\bullet}$ and H_2O_2 were detected in the present system, the intermediates superoxide radicals ($O_2^{\bullet -}$ and $HO_2^{\bullet}$) should also exist and contribute to the microbial inactivation process.

Further verification of the visible light mediated photocatalysis processes was conducted by the characterization of Ag-NPs@CTA by X-ray photoelectron spectroscopy (XPS) and UV–vis adsorption spectrometry. XPS was used to study the chemical state of Ag-NPs and TiO_2 and the results were shown in Fig. 5a and Fig. 5b. In the Ti2p XPS spectrum of CTA, the two peaks at 458.5 eV and 464.15 eV ascribed to $Ti2p_{3/2}$ and $Ti2p_{1/2}$, respectively, indicating Ti was in the state of Ti^{4+} [59]. While for the Ti2p XPS spectrum of Ag-NPs@CTA, the binding energy of $Ti2p_{3/2}$ and $Ti2p_{1/2}$ was 459.1 eV and 464.25 eV, respectively. The binding energy of Ti2p increased after Ag-NPs loading illustrating the Ti in Ag-NPs@CTA possessed lower electron density [60]. As shown in Fig. 5b, the weak peaks at 368.5 and 374.5 eV could be attributed to Ag3d, and the energy spacing of two lines was 6.0 eV, which was the characteristic peaks of metal Ag indicating Ag exists in the form of Ag^0 [61]. Then, the visible light absorption ability of Ag-NPs@CTA was studied with CTA as control and the results were shown in Fig. 5c. Compared with CTA, Ag-NPs@CTA showed enhanced visible light absorption ability with an absorption peak at 432 nm resulting from the surface plasmonic resonance of Ag nanoparticles. The characterization results proved that visible light could activate the Ag nanoparticles to generate electrons which could migrate to their neighbor TiO_2 and result in subsequent photocatalytic reactions (Eqs. (1)–(6)).

Fig. 6 summarized the synergistic antimicrobial mechanism of Ag-NPs@CTA toward microbial cells under visible light irradiation:

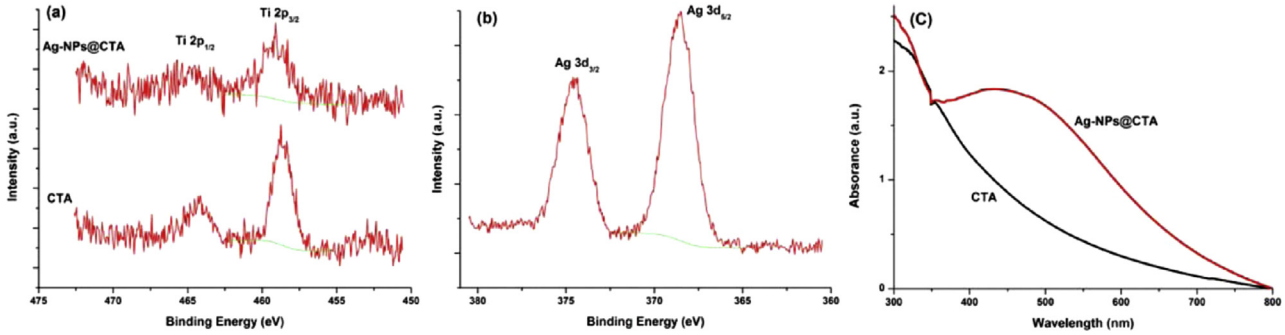

Fig. 5. (a) Ti2p high-resolution XPS spectra of CTA and Ag-NPs@CTA samples. (b) Ag3d high-resolution XPS spectrum of Ag-NPs@CTA. (c) UV–vis absorption spectra of Ag-NPs@CTA and blank CTA membranes.

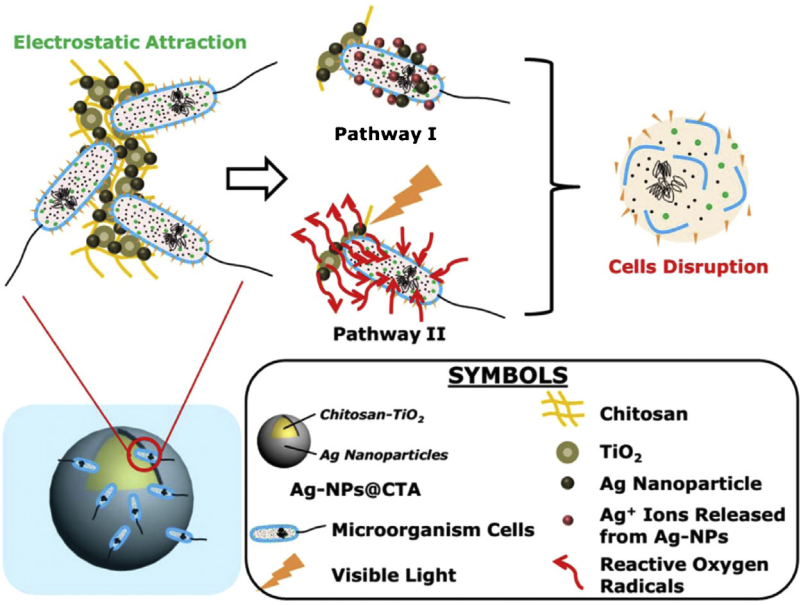

Fig. 6. Proposed antimicrobial mechanism.

Firstly, negative charged cells could attach to the positive surface of Ag-NPs@CTA (from polycationic chitosan and chemisorbed Ag^+ ions on the Ag-NPs surface) by electrostatic attraction. This process could not only inhibit the growth of cells but also facilitate the performance of the further toxicity effects which contained the following two pathways: (I) free Ag species (Ag^+ and Ag-NPs/Ag^+) released from Ag nanoparticles bound to the cell membrane to cause penetration change and then enter intracellular environment resulting in metabolic dysfunction and interrupt of DNA replication; (II) holes (h^+) and reactive oxygen radicals ($O_2^{\bullet -}$, $OH^\bullet$, $HO_2^\bullet$, H_2O_2) generated from the visible light mediated photocatalysis reactions degrade substances of cell wall and membrane; thereby, leading to the disruption of cells and intracellular substances leakage.

When UV light was used, the antimicrobial mechanism of Ag-NPs@CTA was similar with that under visible light only with the differences in the light induced charge separation process on the surface of the composite. Under visible light irradiation, electrons were first generated on the surface of Ag nanoparticles by the localized surface plasmonic resonance (LSPR) effect and then transferred to their neighbor TiO_2 to trigger the charge separation and the following photocatalytic reactions. While under UV light irradiation, Ag nanoparticles could absorb UV light by interband excitation of electrons from 4d to 5sp and more activated electrons generated than through SPR effect [62]. Furthermore, UV light could also activate TiO_2 to generate holes and electrons by charge separation process. So, under UV light irradiation, more free electrons could generate and transfer to the adsorbed oxygen molecules to produce reactive oxygen species which contributed directly to inactivate microbial cells. And that was why Ag-NPs@CTA showed the highest antimicrobial activity under UV light irradiation as discussed in Section 3.1 (Fig. 1c).

4. Conclusions

In summary, Ag-NPs@CTA exhibited a great potential for portable water disinfection because of its efficient antimicrobial effects under visible light irradiation, satisfactory reusability and low cytotoxicity for mammalian cells. Ag-NPs@CTA treatment could not only lead to the destruction of cell wall and membrane and intracellular substances leakage but could also affect the microbial substances metabolism processes. The enhanced antimicrobial activities originated from the synergistic effects of the three components containing electrostatic interaction followed by free Ag species toxicity and oxidative stress from the photo-generated reactive radicals. This paper provided a new idea in designing visible light activated photocatalytic antimicrobial agents for water disinfection and developed a realistic method in the antimicrobial mechanism study.

Acknowledgements

The authors want to express their thanks for the supports from National Basic Research Program (973 Program) of China (2014CB745100), the (863) High Technology Project (2012AA021402), the Project sponsored by SRF for ROCS, SEM (LXJJ2012-001), and the Chinese Universities Scientific Fund(JD1417).

Appendix A. Supplementary data

Supplementary data associated with this article can be found, in the online version, at http://dx.doi.org/10.1016/j.apcatb.2015.01.042.

References

[1] M.A. Shannon, P.W. Bohn, M. Elimelech, J.G. Georgiadis, B.J. Marinas, A.M. Mayes, Nature 452 (2008) 301–310.
[2] S. Pigeot-Rémy, F. Simonet, E. Errazuriz-Cerda, J.C. Lazzaroni, D. Atlan, C. Guillard, Appl. Catal. B: Environ. 104 (2011) 390–398.
[3] World Health Organization (WHO), Emerging Issues in Water and Infectious Disease, World Health Organization (WHO), Geneva, 2003.
[4] World Health Organization (WHO), Volume Guidelines for Drinking-Water Quality, 1, third ed., World Health Organization (WHO), Geneva, 2008.
[5] C.A. Martínez-Huitle, E. Brillas, Angew. Chem. Int. Ed. 47 (2008) 1998–2005.
[6] C.H. Deng, J.L. Gong, G.M. Zeng, C.G. Niu, Q.Y. Niu, W. Zhang, H.Y. Liu, J. Hazard. Mater. 276 (2014) 66–76.
[7] G.A. Boorman, Environ. Health Perspect. 107 (1999) 207–217.
[8] Y. Zhang, Y. Zhu, J. Yu, D. Yang, T.W. Ng, P.K. Wong, J.C. Yu, Nanoscale 5 (2013) 6307–6310.
[9] S.W. Krasner, H.S. Weinberg, S.D. Richardson, S.J. Pastor, R. Chinn, M.J. Sclimenti, G.D. Onstad, A.D. Thruston Jr., Environ. Sci. Technol. 40 (2006) 7175–7185.
[10] Y.-T. Woo, D. Lai, J.L. McLain, M.K. Manibusan, V. Dellarco, Environ. Health Perspect. 110 (2002) 75–88.
[11] J. Marugán, R. van Grieken, C. Sordo, C. Cruz, Appl. Catal. B: Environ. 82 (2008) 27–36.
[12] D. Venieri, A. Fraggedaki, M. Kostadima, E. Chatzisymeon, V. Binas, A. Zachopoulos, G. Kiriakidis, D. Mantzavinos, Appl. Catal. B: Environ. 154–155 (2014) 93–101.
[13] A. Alonso, X. Muñoz-Berbel, N. Vigués, R. Rodríguez-Rodríguez, J. Macanás, M. Muñoz, J. Mas, D.N. Muraviev, Adv. Funct. Mater. 23 (2013) 2450–2458.
[14] A. Fujishima, K. Honda, Nature 238 (1972) 37–38.
[15] A.L. Giraldo, G.A. Penuela, R.A. Torres-Palma, N.J. Pino, R.A. Palominos, H.D. Mansilla, Water Res. 44 (2010) 5158–5167.
[16] K. Pathakoti, S. Morrow, C. Han, M. Pelaez, X. He, D.D. Dionysiou, H. Hwang, Environ. Sci. Technol. 47 (2013) 9988–9996.
[17] T. Matsunaga, R. Tomoda, T. Nakajima, H. Wake, FEMS Microbiol. Lett. 29 (1985) 211–214.
[18] J. Zhang, Y. Liu, Q. Li, X. Zhang, J.K. Shang, ACS Appl. Mater. Interfaces 5 (2013) 10953–10959.
[19] C.M. Davies, D.J. Roser, A.J. Feitz, N.J. Ashbolt, Water Res. 43 (2009) 643–652.
[20] S.W. Verbruggen, M. Keulemans, M. Filippousi, D. Flahaut, G. Van Tendeloo, S. Lacombe, J.A. Martens, S. Lenaerts, Appl. Catal. B: Environ. 156–157 (2014) 116–121.
[21] H. Zhang, X. Fan, X. Quan, S. Chen, H. Yu, Environ. Sci. Technol. 45 (2011) 5731–5736.
[22] K. Naoi, Y. Ohko, T. Tatsuma, J. Am. Chem. Soc. 126 (2004) 3664–3668.
[23] T. Wu, K. Wang, G. Li, S. Sun, J. Sun, J. Chen, ACS Appl. Mater. Interfaces 2 (2010) 544–550.
[24] W. Su, S.S. Wei, S.Q. Hu, J.X. Tang, J. Hazard. Mater. 172 (2009) 716–720.
[25] A. Sclafani, M. Mozzanega, J. Herrmann, J. Catal. 168 (1997) 117–120.
[26] Q. Zhang, C. Sun, Y. Zhao, S. Zhou, X. Hu, P. Chen, Environ. Sci. Technol. 44 (2010) 8270–8275.
[27] I.M. Butterfield, P.A. Christensen, A. Hamnett, K.E. Shaw, G.M. Walker, S.A. Walker, C.R. Howarth, J. Appl. Electrochem. 27 (1997) 385–395.
[28] P. Lei, F. Wang, X. Gao, Y. Ding, S. Zhang, J. Zhao, S. Liu, M. Yang, J. Hazard. Mater. 227–228 (2012) 185–194.
[29] S. Matsuzawa, C. Maneerat, Y. Hayata, T. Hirakawa, N. Negishi, T. Sano, Appl. Catal. B: Environ. 83 (2008) 39–45.
[30] J. Zeng, S. Liu, J. Cai, L. Zhang, J. Phys. Chem. C 114 (2010) 7806–7811.
[31] X. Zhang, M. Hejazi, S.J. Thiagarajan, W.R. Woerner, D. Banerjee, T.J. Emge, W. Xu, S.J. Teat, Q. Gong, A. Safari, R. Yang, J.B. Parise, J. Li, J. Am. Chem. Soc. 135 (2013) 17401–17407.
[32] E.I. Rabea, M.E. Badawy, C.V. Stevens, G. Smagghe, W. Steurbaut, Biomacromolecules 4 (2003) 1457–1465.
[33] H. Tang, P. Zhang, T.L. Kieft, S.J. Ryan, S.M. Baker, W.P. Wiesmann, S. Rogelj, Acta Biomater. 6 (2010) 2562–2571.
[34] M. Banerjee, S. Mallick, A. Paul, A. Chattopadhyay, S.S. Ghosh, Langmuir 26 (2010) 5901–5908.
[35] L. Mei, Z. Lu, W. Zhang, Z. Wu, X. Zhang, Y. Wang, Y. Luo, C. Li, Y. Jia, Biomaterials 34 (2013) 10328–10337.
[36] E. Chen, H. Su, T. Tan, J. Chem. Technol. Biotechnol. 86 (2011) 421–427.
[37] H.R. Barbosa, M.F.A. Rodrigues, C.C. Campos, M.E. Chaves, I. Nunes, Y. Juliano, N.F. Novo, J. Microbiol. Methods 22 (1995) 39–50.
[38] X. Lü, D. Li, Y. Huang, Y. Zhang, Surf. Coat. Technol. 201 (2007) 6843–6846.
[39] T. Fujimoto, Y. Tsuchiya, M. Terao, K. Nakamura, M. Yamamoto, Int. J. Food Microbiol. 112 (2006) 96–101.
[40] T. Qian, H. Su, T. Tan, J. Photochem. Photobiol. A 218 (2011) 130–136.
[41] B. Xi, X. Chu, J. Hu, C.S. Bhatia, A.J. Danner, H. Yang, Appl. Surf. Sci. 311 (2014) 582–592.
[42] T.A. Camesano, M.J. Natan, B.E. Logan, Langmuir 16 (2000) 4563–4572.
[43] P. Kao, N.A. Malvadkar, M. Cetinkaya, H. Wang, D.L. Allara, M.C. Demirel, Adv. Mater. 20 (2008) 3562–3565.
[44] J.W. Chan, H. Winhold, M.H. Corzett, J.M. Ulloa, M. Cosman, R. Balhorn, T. Huser, Cytom. Part A 71A (2007) 468–474.
[45] L. Cui, P. Chen, S. Chen, Z. Yuan, C. Yu, B. Ren, K. Zhang, Anal. Chem. 85 (2013) 5436–5443.
[46] Y. Wang, K. Lee, J. Irudayaraj, J. Phys. Chem. C 114 (2010) 16122–16128.
[47] M. Kahraman, M.M. Yazıcı, F. Şahin, M. Çulha, Langmuir 24 (2008) 894–901.
[48] J. Sundaram, B. Park, Y. Kwon, K.C. Lawrence, Int. J. Food Microbiol. 167 (2013) 67–73.
[49] D. Helm, H. Labischinski, G. Schallehn, D. Naumann, J. Gen. Microbiol. 137 (1991) 69–79.
[50] J.J. Ojeda, M.E. Romero-González, R.T. Bachmann, R.G.J. Edyvean, S.A. Banwart, Langmuir 24 (2008) 4032–4040.
[51] G. Xiao, X. Zhang, H. Su, T. Tan, Bioresour. Technol. 143 (2013) 490–498.
[52] V. Ambrogi, A. Donnadio, D. Pietrella, L. Latterini, F.A. Proietti, F. Marmottini, G. Padeletti, S. Kaciulis, S. Giovagnoli, M. Ricci, J. Mater. Chem. B 2 (2014) 6054–6063.
[53] N.S. Wigginton, A.D. Titta, F. Piccapietra, J. Dobias, V.J. Nesatyy, M.J.F. Suter, R. Bernier-Latmani, Environ. Sci. Technol. 44 (2010) 2163–2168.
[54] K.B. Holt, A.J. Bard, Biochemistry 44 (2005) 13214–13223.
[55] K. Chaloupka, Y. Malam, A.M. Seifalian, Trends Biotechnol. 28 (2010) 580–588.
[56] E.M. Rodríguez, G. Márquez, M. Tena, P.M. Álvarez, F.J. Beltrán, Appl. Catal. B: Environ. (2014) http://dx.doi.org/10.1016/j.apcatb.2014.11.002
[57] G.T. Li, K.H. Wong, X.W. Zhang, C. Hu, J.C. Yu, R.C.Y. Chan, P.K. Wong, Chemosphere 76 (2009) 1185–1191.
[58] N. Zhang, S.Q. Liu, X.Z. Fu, Y.J. Xu, J. Phys. Chem. C 115 (2011) 9136–9145.
[59] W. Wang, D. Wang, W. Qu, L. Lu, A. Xu, J. Phys. Chem. C 116 (2012) 19893–19901.
[60] Y. Shiraishi, H. Sakamoto, K. Fujiwara, S. Ichikawa, T. Hirai, ACS Catal. 4 (2014) 2418–2425.
[61] H. Shi, J. Chen, G. Li, X. Nie, H. Zhao, P. Wong, T. An, ACS Appl. Mater. Interfaces 5 (2013) 6959–6967.
[62] X. Chen, Z. Zheng, X. Ke, E. Jaatinen, T. Xie, D. Wang, C. Guo, J. Zhao, H. Zhu, Green Chem. 12 (2010) 414–419.